models of biological membranes and in other applications. The observation of spontaneous multilayer formation suggests new ways for selective formation of multilayers versus monolayers, such as the use of molecules containing hydrophobic chains with hydrophilic groups at each end. The lateral and interlayer packing of these multilayers should be controllable through the use of amphiphilic tailor-made additives in a manner similar to that described in this report.

## REFERENCES AND NOTES

1. I. Weissbuch, L. Addadi, M. Lahav, L. Leiserowitz, *Science* **253**, 637 (1991).
2. D. Zbaida *et al.*, *React. Polym.* **6**, 241 (1987).
3. E. Staab, L. Addadi, L. Leiserowitz, M. Lahav, *Adv. Mater.* **2**, 40 (1990).
4. The synchrotron radiation beam was monochromated to a wavelength of 1.35 Å at HASYLAB and 1.38 Å at ESRF. To maximize surface sensitivity, we adjusted the beam to strike the sample at an incident angle of $\alpha_f = 0.85\alpha_c$, where $\alpha_c \approx 0.14°$ is the critical angle for total external reflection. The dimensions of the incoming x-ray beam on the liquid surface were 50 mm by 2.5 mm. Several types of information are collected by the position sensitive detector (PSD), which has its axis along the vertical direction $z$. The scattered intensity measured by scanning different values of $q_{xy}$ ($\approx 4\pi\sin\theta/\lambda$) and integrating over the whole $q_z$ window of the PSD ($q_z = 2\pi\sin\alpha_f/\lambda$, where $\alpha_f$ is the angle between the water surface and the scattered beam) yields Bragg peaks. Because there is no selection rule or restriction along $q_z$, the GID patterns arise from a two-dimensional array of rods, called Bragg rods, which extend parallel to the vector $q_z$. The scattered intensity recorded in channels along the PSD but integrated in $q_{xy}$ across a Bragg peak produces $q_z$-resolved scans called Bragg rod profiles. Schematic diagrams of the GID setup are given in (*5*, *6*).
5. J. Als-Nielsen and K. Kjaer, in *Proceedings of the NATO Advanced Study Institute: Phase Transitions in Soft Condensed Matter*, T. Riste and D. Sherrington, Eds. (Plenum, New York, 1989), p. 113.
6. D. Jacquemain *et al.*, *Angew. Chem. Int. Ed. Engl.* **31**, 130 (1992), and references therein.
7. J. Als-Nielsen, in *Handbook on Synchrotron Radiation*, G. S. Brown and D. E. Moncton, Eds. (North-Holland, Amsterdam, 1991), vol. 3, pp. 471–503.
8. S. P. Weinbach *et al.*, *J. Am. Chem. Soc.* **115**, 11110 (1993).
9. Arachidic acid (Sigma; purity, 99%) was converted into arachidamide or NMA in two steps: the formation of the chloride derivative by action of $SOCl_2$ followed by treatment with ammonia for the primary amide or methylamine for the secondary amide. Purities were checked by thin layer chromatography. The identities of the compounds were checked by nuclear magnetic resonance and infrared spectroscopies. Spreading solutions were prepared in chloroform (Merck, analytical grade) with concentrations close to $5 \times 10^{-4}$ M.
10. The correlation length, $L \approx 0.90 \times 2\pi/(\mathrm{FWHM}^2 - \Delta^2)^{1/2}$, where FWHM is the full width at half maximum of the Bragg peak and Δ is the resolution FWHM, associated with the GID $\{h,k\}$ reflection corresponds to the average length of all diffracting crystallites over which "perfect" crystallinity extends in the direction of the reciprocal lattice vector $\mathbf{d}^*_{hk}$.
11. A. Guinier, *X-ray Diffraction* (Freeman, San Francisco, CA, 1968).
12. The approximate thickness $T$ of the crystalline film (in angstroms) is given by $0.9\ [2\pi/\mathrm{FWHM}(Q_z)]$, where $\mathrm{FWHM}(Q_z)$ is the FWHM of the Bragg rod in reciprocal angstroms.
13. The sharp peak observed at around $q_z = 0.01$ Å$^{-1}$ is caused by the interference of rays diffracted up with rays diffracted down and subsequently reflected back up by the interface (*14*).
14. G. Vineyard, *Phys. Rev. B* **26**, 4146 (1982).
15. K. Kjaer, J. Als-Nielsen, C. A. Helm, P. Tippman-Krayer, H. Möhwald, *J. Phys. Chem.* **93**, 3200 (1989).
16. S. P. Weinbach, K. Kjaer, J. Als-Nielsen, M. Lahav, L. Leiserowitz, *ibid.* **97**, 5200 (1993).
17. Several high order reflections were also observed, although not all $q_{xy}$ values were measured. Those found were the $\{1,2\} + \{1,\bar{2}\}$ ($q_{xy} = 2.11$ Å$^{-1}$), $\{2,0\}$ (2.53 Å$^{-1}$), $\{2,1\} + \{2,\bar{1}\}$ (2.67 Å$^{-1}$), and the $\{1,3\} + \{1,\bar{3}\}$ (2.85 Å$^{-1}$) reflections. The region of the $\{0,1\}$ reflection, calculated to be at $q_{xy} = 0.85$ Å$^{-1}$, was not measured.
18. During an earlier measurement at the bending magnet beamline (*16*), two reflections were observed for arachidamide over formamide. These were interpreted as a single phase composed of a trilayer with the molecules vertically oriented with respect to the liquid surface. Closer inspection of the earlier GID pattern reveals that the additional reflections were in fact present but were of such low intensity that they were not noticed.
19. The tilt, $t$, of the molecules is given by $\tan t \cos \Psi_{hk} = q_z^0/q_{hk}$, where $q_z^0$ is the maximum position of the Bragg rod along $q_z$, $q_{hk}$ is the position of the $hk$ reflection in $q_{xy}$, and $\Psi_{hk}$ is the angle between the direction of tilt as projected onto the horizontal plane and the reciprocal lattice vector $hk$ (*5*).
20. These dimensions are similar to those found for the diamide APA over water subphase (*8*).
21. The $\{2,1\} + \{2,\bar{1}\}$ ($q_{xy} = 2.49$ Å$^{-1}$) and $\{1,2\} + \{1,\bar{2}\}$ (2.61 Å$^{-1}$) reflections were also measured.
22. We may describe the structure in terms of the pseudorectangular cell $\mathbf{a}' = \mathbf{a} + \mathbf{b} = 4.21$ Å and $\mathbf{b}' = \mathbf{a} - \mathbf{b} = 9.13$ Å, with $\gamma' = 93.2°$. The unusually long $\mathbf{b}'$ axis is strongly indicative that the plane passing through the hydrocarbon backbone is parallel to the axis $\mathbf{b}'$ (Fig. 4), as has been seen in 3D crystal structures of α,ω-diamides (*23*). The chains of the two molecules in the unit cell are therefore likely to be parallel to one another. Thus, we may describe the structure in terms of the oblique unit cell $\mathbf{a},\mathbf{b},\gamma$ with one molecule per unit cell, and all molecules in the crystal are related by translation.
23. P. M. Hospital, *Acta Crystallogr. B* **27**, 484 (1971),
24. J. D. Turner and E. C. Lingafelter, *Acta Crystallogr.* **8**, 549 (1955); *ibid.*, p. 551.
25. A monolayer of amphiphilic molecules at the air-liquid interface may be regarded as a different phase than a multilayer with the same intralayer packing mode. A monolayer contains essentially three sets of intermolecular interactions, namely the intralayer interactions between molecules, the interaction between the polar head group and the subphase, and that of the terminal methyl with the air. The corresponding multilayer contains these same interactions plus two additional contacts: the interlayer head-to-head contacts between polar head groups and the interlayer contacts between terminal methyl groups.
26. L. Addadi *et al.*, *Angew. Chem. Int. Ed. Engl.* **24**, 466 (1985).
27. M. Lahav and L. Leiserowitz, *J. Phys. D* **26**, B22 (1993).
28. K. Lewtas, R. D. Tack, D. H. M. Beiny, J. W. Mullin, in *Advances in Industrial Crystallization*, J. Garside, R. J. Davey, A. G. Jones, Eds. (Butterworth-Heinemann, Oxford, 1991), p. 166.

29. We thank E. Shavit for the syntheses of the additive materials and F. Leveiller and D. Jacquemain for assistance with the GID measurements. We acknowledge financial support from The Minerva Foundation, Munich, the Israel Academy of Science and Humanities, and the Danish Foundation for Natural Sciences. We also acknowledge HASYLAB, DESY, Hamburg, and ESRF, Grenoble, for beam time.

24 January 1994; accepted 14 April 1994

---

# New Phases of $C_{60}$ Synthesized at High Pressure

Y. Iwasa,* T. Arima, R. M. Fleming, T. Siegrist, O. Zhou,
R. C. Haddon, L. J. Rothberg, K. B. Lyons, H. L. Carter Jr.,
A. F. Hebard, R. Tycko, G. Dabbagh, J. J. Krajewski,
G. A. Thomas, T. Yagi

**The fullerene $C_{60}$ can be converted into two different structures by high pressure and temperature. They are metastable and revert to pristine $C_{60}$ on reheating to 300°C at ambient pressure. For synthesis temperatures between 300° and 400°C and pressures of 5 gigapascals, a nominal face-centered-cubic structure is produced with a lattice parameter $a_o = 13.6$ angstroms. When treated at 500° to 800°C at the same pressure, $C_{60}$ transforms into a rhombohedral structure with hexagonal lattice parameters of $a_o = 9.22$ angstroms and $c_o = 24.6$ angstroms. The intermolecular distance is small enough that a chemical bond can form, in accord with the reduced solubility of the pressure-induced phases. Infrared, Raman, and nuclear magnetic resonance studies show a drastic reduction of icosahedral symmetry, as might occur if the $C_{60}$ molecules are linked.**

Although $C_{60}$ molecules are extremely stable at ambient conditions, nonhydrostatic compression induces a transformation of $C_{60}$ to diamond (*1*) or unknown structures above 15 GPa (*2*–*4*). Light irradiation is also reported to cause a polymerization (*5*). We have found at least two crystalline phases of carbon involving crosslinked $C_{60}$ cages that can be synthesized from pure $C_{60}$.

Synthesis was performed at high pressure and high temperature with a wedge-type cubic anvil apparatus (*6*), which produces quasi-hydrostatic pressure. About 20 mg of $C_{60}$ was pressed into a pellet and sandwiched between two Ti-powder oxygen get-

---

Y. Iwasa, R. M. Fleming, T. Siegrist, O. Zhou, R. C. Haddon, L. J. Rothberg, K. B. Lyons, H. L. Carter Jr., A. F. Hebard, R. Tycko, G. Dabbagh, J. J. Krajewski, G. A. Thomas, AT&T Bell Laboratories, Murray Hill, NJ 07974, USA.
T. Arima, Department of Physics, University of Tokyo, Tokyo 113, Japan.
T. Yagi, Institute for Solid State Physics, University of Tokyo, Tokyo 106, Japan.

---

*On leave from the Department of Applied Physics, University of Tokyo, Tokyo 113, Japan.

**Table 1.** Lattice parameters of pristine $C_{60}$ and the pressure-induced phases of $C_{60}$.

| Phase | Cubic | Hexagonal | | Volume per $C_{60}$ molecule ($Å^3$) |
|---|---|---|---|---|
| | $a_0$ (Å) | $a_0$ (Å) | $c_0$ (Å) | |
| Pristine fcc | 14.17 | 10.02 | 24.54 | 711 |
| fcc($pC_{60}$) | 13.6 | 9.62 | 23.6 | 629 |
| rh($pC_{60}$) | — | 9.22 | 24.6 | 603 |

ters, which were loaded into a gold capsule 4.5-mm in diameter and 10 mm in length. The capsule was placed in a dry box to minimize the exposure of $C_{60}$ to air. This capsule was surrounded by a cylindrical graphite heater enclosed inside an insulating NaCl spacer. Pyrophyllite was used as a pressure medium.

The pressure and temperature were applied in steps. First, the pressure was increased to 5 GPa over a 1-hour period. The temperature was then ramped for 20 min and held for 1 hour. Subsequently, the temperature was quenched to room temperature in 5 s, followed by a gradual pressure release over 1 hour. The sample was not exposed to air until after the reaction. The reacted sample formed a solid ingot with a clear interface between $C_{60}$ and Ti. Although there was no observable reaction of $C_{60}$ with Ti, we removed the interface region from the ingot before sample characterization.

To rule out the effects of solvent or impurities, we repeated the experiments with three different starting materials, which were (i) chromatographically purified, (ii) purified and vacuum-dried at 200°C for several hours, or (iii) purified, dried, and sublimed. The same results were obtained for all three preparations; however, the x-ray diffraction (XRD) pattern of the pressure-induced phase obtained from the sublimed powders showed the smallest line widths. To check for possible oxygen effects after high-pressure treatment, we placed the sample in a sealed quartz capillary within a He glove box before measuring XRD patterns. The subsequent x-ray data were the same as those taken in air. Based on these results, we conclude that the observed pressure-induced effects are intrinsic to $C_{60}$.

High-pressure synthesis was performed at 100°C steps from 300° to 800°C at fixed pressure $P = 5$ GPa. We obtained CuK$\alpha$ XRD powder patterns (Fig. 1) for pristine $C_{60}$, a sample treated at $P = 5$ GPa and 300°C, and a sample treated at $P = 5$ GPa and 800°C. Whereas ground powders of pristine $C_{60}$ typically show slight broadening over instrumental resolution, both pressure-treated materials show gross broadening, indicating that crystalline order only extends over ~50 to 100 Å in these samples. Despite the broadening, both of the pressure-treated samples can be indexed as single phase.

The 300°C sample is typical of material synthesized between 300° and 400°C and is designated fcc($pC_{60}$). The powder pattern can be indexed as face-centered-cubic (fcc) with a lattice parameter of 13.6 Å, a contraction of ~3.7% from the pristine $C_{60}$ value [this unit cell is larger than the 5-GPa in situ value reported by Duclos *et al.* (2)]. The solid line through the 300°C data in Fig. 1 is the result of a calculation done with LAZY-PULVERIX (7) in which the $C_{60}$ molecule was replaced by a spherical shell of charge with a radius of 3.5 Å. To accurately fit the positions of the observed maxima in the powder pattern, it is necessary to use the form factor for the spherical shell, $\sin(qR)/qR$, where $R$ is the $C_{60}$ diameter and $q$ is the momentum transfer, when calculating the shape of broadened peaks. In regions where the form factor is rapidly varying, such as near the (200) peak, the observed peak position can be noticeably shifted from the calculated position. One can obtain a fit that is nearly as good by using the same rhombohedral model used in the high-temperature phase, but with broader peaks. We have chosen not to describe our data with the rhombohedral model because we do not observe splitting of the peak near $2\theta = 18°$. In addition, spectroscopy data reported below indicate that the local environment of the $C_{60}$ molecule is different in the two phases.

For samples prepared at temperatures between 500° and 800°C, a noncubic symmetry is observed in room-temperature XRD patterns [a similar phase has been reported by Bethoux *et al.* (8)]. We found that this pattern can be indexed as rhombohedral symmetry with hexagonal lattice parameters of $a_0 = 9.22$ Å and $c_0 = 24.6$ Å. We denote this phase as rh($pC_{60}$) with a primitive rhombohedral cell of $a_0 = 9.77$ Å and $\alpha = 56.3°$. The solid line through the 800°C data in Fig. 1 is the result of a LAZY-PULVERIX calculation with the space group $R\bar{3}m$. The model contains a single sphere at the origin [the symmetry results in three equivalent molecules per hexagonal cell at (0,0,0), (⅓,⅔,⅓), and (⅔,⅓,⅔)].

The rh($pC_{60}$) structure can be thought of as a distortion of fcc structure resulting from an elongation along [111]. The model qualitatively describes the data and correctly predicts the systematic absences but fails to predict the detailed structure of the data, particularly at higher angles. A Rietveld refinement in which the spherical shell model is used does not produce a significant improvement of the fit. This is to be expected because spectroscopy data indicate that the $C_{60}$ molecules lose their icosahedral $I_h$ symmetry in both pressure-induced phases. In these phases, a spherical shell of charge will be inadequate in describing the detailed charge distribution of the molecule that is expected to be nonspherical. Although in principle one could attempt to model the distorted $C_{60}$ molecule with in-

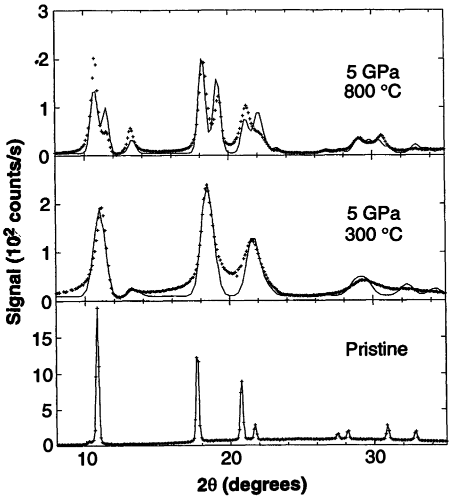

**Fig. 1.** The x-ray diffraction patterns for pristine fcc $C_{60}$ and high-pressure forms synthesized at the indicated conditions. Crosses and solid lines are experimental points and patterns calculated with the spherical shell model, respectively.

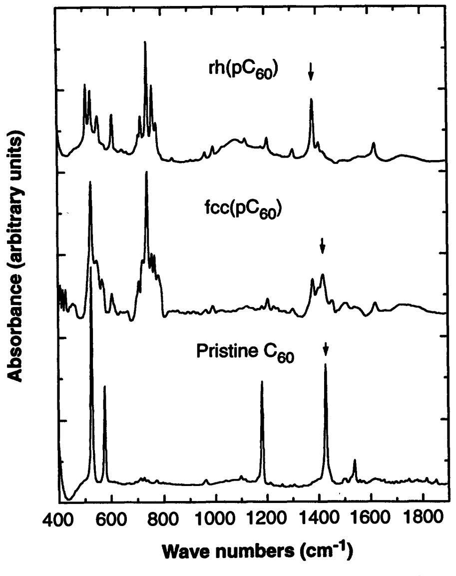

**Fig. 2.** Infrared absorption spectra of powders dispersed in KBr pellets for pristine $C_{60}$, fcc($pC_{60}$), and rh($pC_{60}$). The background was subtracted. Arrows indicate the strongest peak in the C=C stretching vibration region.

dividual carbon atoms, it is unlikely that such a model will yield a stable refinement unless the quality of the x-ray data improves significantly.

In each structure, the nearest intermolecular distance is given by the hexagonal cell parameter, $a_o$. The two close-packed cubic structures have isotropic nearest neighbor distances with 12 nearest neighbors (Table 1). The rhombohedral structure is anisotropic with six nearest-neighbors (9.22 Å) in the "waist" [the old fcc (111) plane] and six next nearest neighbors (9.76 Å) above and below the waist. Although the volume per molecule monotonically decreases as the synthesis temperature increases (Table 1), the hexagonal $c_0$ axis goes through a minimum in the isotropic fcc(p$C_{60}$) structure and increases in the anisotropic rhombohedral phase.

We measured the powder infrared (IR) absorption spectra for pristine $C_{60}$, fcc(p$C_{60}$), and rh(p$C_{60}$) (Fig. 2). Only four strong absorption peaks are observed in pristine $C_{60}$. In sharp contrast, the spectra for two pressurized forms have substantially richer structures, indicating a significant reduction of $I_h$ symmetry. Most of the peaks observed in the spectrum of pristine $C_{60}$ are either split or shifted in the other spectra. Both pressure-induced forms show several intense peaks near 700 to 800 $cm^{-1}$, a region that is featureless for pristine $C_{60}$. Similar IR spectra are observed when the $C_{60}$ skeleton is partly broken, for instance, as in the case of the epoxide $C_{60}O$ (9) and photopolymerized $C_{60}$ (5). Considering the similar nature of the IR absorption spectra, intermolecular chemical bondings or strong distortions in molecules are present in both fcc(p$C_{60}$) and rh(p$C_{60}$).

One of the other notable features in the IR spectra is the softening of the strongest peak in the C=C stretching vibration region (indicated by arrows in Fig. 2). Although this mode is observed at 1428 $cm^{-1}$ in pristine $C_{60}$, it is shifted to 1422 $cm^{-1}$ and 1383 $cm^{-1}$ for fcc(p$C_{60}$) and rh(p$C_{60}$), respectively. The position of this mode is known to be very sensitive to the degree of charge transfer on the $C_{60}$ molecule and to the polymerization of $C_{60}$. For example, it is observed at 1341 $cm^{-1}$ for $K_6C_{60}$ (*10*) and at 1424 $cm^{-1}$ in photopolymerized $C_{60}$ (5). The observed shift of 45 $cm^{-1}$ in rh(p$C_{60}$) is significantly large, especially when one considers that the material is undoped. The IR data for the two pressure-induced phases show the same trend as that seen in the photopolymerized $C_{60}$. If we assume that the position of this band reflects the strength of the intermolecular bonding, the order of these phases on the basis of increasing bond strength is photopolymerized $C_{60}$, fcc(p$C_{60}$), then rh(p$C_{60}$).

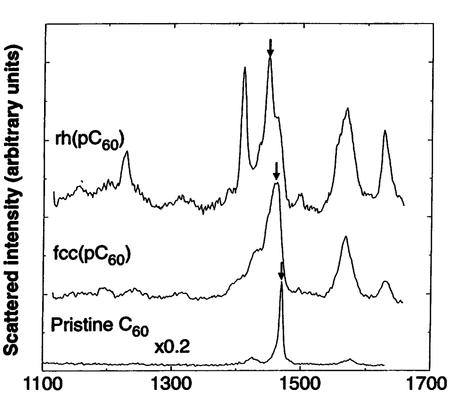

**Fig. 3.** Raman scattering spectra of pristine $C_{60}$, fcc(p$C_{60}$), and rh(p$C_{60}$). The pristine $C_{60}$ peak has been reduced to one-fifth of its intensity for scaling purposes. Arrows mark the $C_{60}$ Ag mode.

The Raman spectra for powder samples of pristine $C_{60}$, fcc(p$C_{60}$), and rh(p$C_{60}$) (Fig. 3) were made with an incident laser of 5145 Å at the power of 2 W/$cm^2$, which is small enough to neglect the effects of photoinduced polymerization. Although the peaks are broad, the spectra are richer in both pressure-induced forms than that seen in pristine $C_{60}$. As indicated by arrows, the Ag mode at 1468 $cm^{-1}$ in pristine $C_{60}$ is shifted to 1457 and 1447 $cm^{-1}$ in fcc(p$C_{60}$) and rh(p$C_{60}$), respectively. These trends are similar to those observed in the IR absorption.

A solid-state $^{13}C$ nuclear magnetic resonance (NMR) spectrum was acquired at 100.46 MHz with magic angle spinning. In a marked contrast with a sharp single spectrum for pristine $C_{60}$, a broad peak centered at 125 parts per million was observed together with several subpeaks in both pressure-induced phases, indicating that there exist several inequivalent carbon sites. The IR absorption, Raman scattering, and NMR spectra are consistent with the significant change of the bonding characters and a loss of $I_h$ symmetry in fcc(p$C_{60}$) and rh(p$C_{60}$).

The absorption spectra in the ultraviolet-visible region were measured for powder samples of pristine $C_{60}$, fcc(p$C_{60}$), and rh(p$C_{60}$) dispersed in KBr pellets. The peaks in pristine $C_{60}$ that are attributed to the intramolecular electronic transitions are in good agreement with the data for thin-film samples. In the two pressure-induced forms, the peaks are significantly broadened. The broad features of the peaks are likely attributed to the lifting of the degeneracy of the molecular energy level by the reduction of $I_h$ symmetry.

The solubility of the two pressurized phases were tested in toluene and 1,2-dichlorobenzene, both of which are good solvents for pristine $C_{60}$ (*11*). Neither fcc(p$C_{60}$) nor rh(p$C_{60}$) dissolve in either toluene or 1,2-dichlorobenzene. This result also suggests linked molecule structures in both pressurized forms, in agreement with other experiments.

Although both fcc(p$C_{60}$) and rh(p$C_{60}$) are stable at ambient conditions, they are unstable at high temperatures. In a differential scanning calorimetry (DSC) measurement of rh(p$C_{60}$), an endothermic peak with an enthalpy of 23 J/g was observed upon warming at 270°C. No peak was observed in the cooling scan, indicating an irreversible transition. We characterized the sample after the DSC measurement by XRD and IR absorption. These data show that rh(p$C_{60}$) reverts to the normal fcc $C_{60}$. Although fcc(p$C_{60}$) did not display any well-defined peaks in DSC data, this phase also converted to normal $C_{60}$ after heating. This finding indicates that both fcc(p$C_{60}$) and rh(p$C_{60}$) are metastable phases of $C_{60}$. The recovery of pressurized materials was also reported by Yamawaki *et al.* (*12*) and by Bethoux *et al.* (8) at lower annealing temperatures, indicating that the transition is controlled by kinetics. As a final remark, the XRD pattern of $C_{60}$ pressurized at 1000°C and $P = 5$ GPa was amorphous-like, indicating that under these conditions, the $C_{60}$ molecule decomposed to amorphous carbon.

All of the data presented above clearly show a reconstruction of structures, bondings, and electronic states both in fcc(p$C_{60}$) and rh(p$C_{60}$) suggestive of chemical bonding between neighboring $C_{60}$ molecules. The existence of fcc(p$C_{60}$), rh(p$C_{60}$), and photopolymerized $C_{60}$ suggests that variation of the synthesis conditions might produce a rich variety of other metastable phases containing linked $C_{60}$ molecules.

## REFERENCES AND NOTES

1. M. Núñez Regueiro, P. Monceau, J.-L. Hodeau, *Nature* **355**, 237 (1992).
2. S. J. Duclos, K. Brister, R. C. Haddon, A. R. Kortan, F. A. Thiel, *ibid.* **351**, 380 (1991).
3. M. Núñez Regueiro, P. Monceau, A. Rassat, P. Bernier, A. Zahab, *ibid.* **354**, 289 (1991).
4. F. Moshary *et al.*, *Phys. Rev. Lett.* **69**, 466 (1992).
5. A. M. Rao *et al.*, *Science* **259**, 955 (1993).
6. S. Akimoto, N. Hamaya, I. Shirotani, in *Material Science of the Earth's Interior*, I. Sunagawa, Ed. (Terrapub, Tokyo, 1984), p. 131.
7. K. Yvon, W. Jeitschko, E. Parthe, unpublished software.
8. O. Bethoux, M. Núñez Regueiro, L. Marques, J.-H. Hodeau, M. Perroux, paper presented at the Materials Research Society meeting, Boston, MA, 29 November to 3 December 1993.
9. K. M. Creegan *et al.*, *J. Am. Chem. Soc.* **114**, 1103 (1992).
10. K.-J. Fu *et al.*, *Phys. Rev. B* **46**, 1937 (1992).
11. R. S. Ruoff, D. S. Tse, R. Malhotra, D. C. Lorents, *J. Phys. Chem.* **97**, 3379 (1993).
12. H. Yamawaki *et al.*, *ibid.*, p. 11161.
13. We thank D. W. Murphy and M. Núñez Regueiro for valuable discussions and T. Uchida, T. Hishinuma, and D. H. Rapkine for technical assistance. The work at the University of Tokyo was supported by a Grant-in-Aid for Scientific Research Priority Areas from the Ministry of Education, Science, and Culture, Japan. Y.I. is supported in part by Murata Science Foundation, Japan.

24 February 1994; accepted 23 April 1994